

# Strangeness in Relativistic Astrophysics

JÜRGEN SCHAFFNER-BIELICH

*Institut für Theoretische Physik/Astrophysik, J. W. Goethe Universität, Max-von-Laue-Str. 1, D-60438 Frankfurt/Main, Germany*

STEFAN SCHRAMM

*Center for Scientific Computing and Institut für Theoretische Physik/Astrophysik, J. W. Goethe Universität, Max-von-Laue-Str. 1, D-60438 Frankfurt/Main, Germany*

HORST STÖCKER

*Gesellschaft für Schwerionenforschung, D-64291 Darmstadt, Germany*  
*Frankfurt Institute for Advanced Studies (FIAS), J. W. Goethe Universität, Ruth-Moufang-Str. 1, D-60438 Frankfurt/Main, Germany*  
*Institut für Theoretische Physik/Astrophysik, J. W. Goethe Universität, Max-von-Laue-Str. 1, D-60438 Frankfurt/Main, Germany*

**Summary.** — In these lecture notes, the role of strangeness in relativistic astrophysics of compact stars is addressed. The appearance of strange particles, as hyperons, kaons, and strange quarks, in the core of compact stars is examined and common features as well as differences are presented. Impacts on the global properties of compact stars and signals of the presence of exotic matter are outlined for the various strange phases which can appear in the interior at high densities.

PACS 26.60.+c – Nuclear matter aspects of neutron stars.

PACS 97.60.Jd – Neutron stars.

PACS 21.80.+a – Hypernuclei.

PACS 12.38.Mh – Quark-gluon plasma.

## 1. – Introduction

Neutron stars are the final endpoint in the evolution of stars more massive than eight solar masses. They are born in a spectacular explosive event, a core-collapse supernova, which can outshine an entire galaxy in its brightness. A surprisingly good estimate about the characteristic masses and radii can be made by adopting the argument of Landau [1]. The delicate balance between gravitational energy and Fermi energy can only be achieved up to a certain critical number of nucleons (fermions) which is  $N \approx (M_P/m_N)^3 \approx 10^{57}$ , where  $M_P$  stands for the Planck mass and  $m_N$  for the nucleon mass. The corresponding maximum mass for neutron stars amounts to  $M_{\max} \approx M_p^3/m_N^2 \approx 1.8M_\odot$ . This mass estimate is exactly in the region of maximum masses presently discussed in the literature with much more refined theoretical models of neutron star matter. There are excellent modern textbooks on compact stars available, which discuss the physics of neutron stars and its various phases in great detail. We refer the interested reader to the books by Norman Glendenning [2] and by Fridolin Weber [3] for a thorough treatment of this exciting field in the interplay of physics and astrophysics. Most recently, a new textbook on compact stars appeared which updates and complements the existing ones [4]. A recent review article on the relation between the nuclear equation of state and neutron stars can be found in [5], a nice popular article on neutron stars in [6].

In these lecture notes, we discuss the global properties of neutron stars, masses and radii, and how those change for different compositions in their interior. In particular, we address the appearance of new and exotic phases in dense neutron star matter and how they can modify the mass-radius diagram for compact stars. In section 2, the baryons of the SU(3) octet are treated together in a chiral SU(3) $\times$ SU(3) effective Lagrangian which is motivated from the approximate symmetries of the underlying theory of strong interactions, quantum chromodynamics (QCD). When the properties of hyperons are tied to the known experimental data on hypernuclei, hyperons are present in neutron star matter above twice normal nuclear matter density affecting the properties of massive neutron star configurations. In section 3, strange mesons, the  $K^-$ , and its presence in neutron star matter by forming a Bose-Einstein condensate are addressed. A relativistic field-theoretic approach is utilised to outline the basic features of kaon condensation for compact stars. Ultimately, hadrons have to be described in terms of quark degrees of freedom at high densities. The phase transition from the chirally broken hadronic phase to the approximately chirally restored quark matter phase is examined within perturbative QCD and the MIT bag model to illustrate the main features of a strong first order phase transition in compact star matter in section 4. Characteristics of the mass-radius relation are highlighted which signal the presence of exotic matter in the core of compact stars.

## 2. – Hyperons in Neutron Stars

QCD with massless quarks is chirally symmetric, which means that all left-handed and right-handed quarks decouple. This statement is actually true for all vector interactions.

Left- and right-handed quarks are defined by the relations

$$(1) \quad \begin{aligned} q_L &= \frac{1}{2}(1 - \gamma_5)q & \sim & (3, 0) \\ q_R &= \frac{1}{2}(1 + \gamma_5)q & \sim & (0, 3) \end{aligned} .$$

Splitting a spinor  $\Psi$  to left and right-handed components one gets

$$(2) \quad \bar{\Psi}\gamma_\mu A^\mu \Psi = (\bar{L} + \bar{R})\gamma_\mu A^\mu (L + R) = \bar{L}\gamma_\mu A^\mu L + \bar{R}\gamma_\mu A^\mu R .$$

The mass term for quarks violates chiral symmetry as

$$(3) \quad m\bar{\Psi}\Psi = m(\bar{L} + \bar{R})(L + R) = m(\bar{L}R + \bar{R}L)$$

and quarks with different chirality mix with each other. The explicit breaking of chiral symmetry is small, however, as  $m_{u,d} \approx 10$  MeV and also  $m_s \approx 100$  MeV is much smaller than the nucleon mass  $m_N \approx 1$  GeV so that chiral symmetry is a useful tool. QCD has a complex and nontrivial structure, quark and gluon condensates are present in the vacuum, in particular the light quark condensate  $\sigma$ , the strange quark condensate  $\zeta$  and the gluon condensate  $\chi$ . The nonvanishing vacuum expectation values of these condensates actually generate most of the masses of the hadrons (except for the pseudo-Goldstone bosons).

In constructing an effective chiral Lagrangian for the description of neutron star matter, one has to consider composite quark fields for the meson and baryon fields. First, consider the spin zero mesons. Assuming that they are  $s$ -wave bound states, then the only spinless objects we can form are

$$(4) \quad \bar{q}_R q_L \quad \bar{q}_L q_R \quad .$$

The combinations  $\bar{q}_L q_L$  and  $\bar{q}_R q_R$  vanish, since the left and right chiral subspaces are orthogonal to each other. The resulting representation in chiral  $SU(3) \times SU(3)$  symmetry is then  $(3, 3^*)$  and  $(3^*, 3)$ , respectively. The antiparticles belong to the conjugate representation. Hence, nonets of pseudoscalar and scalar particles have to be considered. For the vector mesons, one has to construct vector-like quantities out of the quark fields  $q_L$  and  $q_R$ . Again assuming  $s$ -wave bound states, the only vectors which can be formed are

$$(5) \quad \bar{q}_L \gamma_\mu q_L \quad \bar{q}_R \gamma_\mu q_R \quad .$$

This suggests assigning the vector and axial vector mesons to the representation  $(3 \times 3^*, 0) \oplus (0, 3 \times 3^*) = (8, 1) \oplus (1, 8)$ , an octet and a singlet state.

The meson fields can be grouped conveniently into matrices under flavour SU(3), here for the scalar fields and pseudoscalar fields

$$(6) \quad \sum_{a=0}^8 (\bar{q}_L \lambda^a q_R + \bar{q}_L \lambda^a \gamma_5 q_R) \equiv \sum_{a=0}^8 (\xi_a \lambda_a + i\pi_a \lambda_a) = \Sigma + i\Pi = M$$

and correspondingly for the vector and axial vector fields as well as for the baryon fields. Out of all these fields one constructs a Lagrangian which obeys the chiral SU(3) symmetry

$$(7) \quad \mathcal{L} = \mathcal{L}_{\text{kin}} + \mathcal{L}_{\text{BM}} + \mathcal{L}_{\text{BV}} + \mathcal{L}_{\text{vec}} + \mathcal{L}_0 + \mathcal{L}_{\text{SB}} + \mathcal{L}_{\text{lep}} ,$$

with the usual kinetic terms for baryons ( $\mathcal{L}_{\text{kin}}$ ), spin-0 fields ( $\mathcal{L}_0$ ), vector mesons ( $\mathcal{L}_{\text{vec}}$ ) and leptons, electrons and muons ( $\mathcal{L}_{\text{lep}}$ ). The baryons couple with Yukawa-type interactions to the spin-0 mesons ( $\mathcal{L}_{\text{BM}}$ ) and to spin-1 mesons ( $\mathcal{L}_{\text{BV}}$ ). An explicit chiral symmetry breaking term is introduced also ( $\mathcal{L}_{\text{SB}}$ ). For homogeneous matter and in the mean-field approximation, derivatives of the boson fields vanish and the fields with unnatural parity (pseudoscalars and axial vector fields) vanish. One arrives at the following expressions for the various terms in the Lagrangian:

$$(8) \quad \begin{aligned} \mathcal{L}_{\text{BM}} + \mathcal{L}_{\text{BV}} &= - \sum_i \bar{\psi}_i [m_i^* + g_{i\omega} \gamma_0 \omega^0 + g_{i\phi} \gamma_0 \phi^0 + g_{N\rho} \gamma_0 \tau_3 \rho_0] \psi_i , \\ \mathcal{L}_{\text{vec}} &= \frac{1}{2} m_\omega^2 \frac{\chi^2}{\chi_0^2} \omega^2 + \frac{1}{2} m_\phi^2 \frac{\chi^2}{\chi_0^2} \phi^2 + \frac{1}{2} \frac{\chi^2}{\chi_0^2} m_\rho^2 \rho^2 + g_4^4 (\omega^4 + 2\phi^4 + 6\omega^2 \rho^2 + \rho^4) , \\ \mathcal{L}_0 &= -\frac{1}{2} k_0 \chi^2 (\sigma^2 + \zeta^2) + k_1 (\sigma^2 + \zeta^2)^2 + k_2 \left( \frac{\sigma^4}{2} + \zeta^4 \right) + k_3 \chi \sigma^2 \zeta \\ &\quad - k_4 \chi^4 - \frac{1}{4} \chi^4 \ln \frac{\chi^4}{\chi_0^4} + \frac{\delta}{3} \ln \frac{\sigma^2 \zeta}{\sigma_0^2 \zeta_0} , \\ \mathcal{L}_{\text{SB}} &= - \left( \frac{\chi}{\chi_0} \right)^2 \left[ m_\pi^2 f_\pi \sigma + (\sqrt{2} m_K^2 f_K - \frac{1}{\sqrt{2}} m_\pi^2 f_\pi) \zeta \right] , \\ \mathcal{L}_{\text{lep}} &= \sum_{l=e,\mu} \bar{\psi}_l [i\gamma_\mu \partial^\mu - m_l] \psi_l . \end{aligned}$$

Nonvanishing vacuum expectation values are generated by spontaneous breaking of chiral symmetry, so there appears a light quark condensate and a strange quark condensate. In addition, effects from the nonvanishing gluon condensate are taken into account by introducing a scalar  $\chi$  field, which is a chiral singlet. These condensates generate the hadron masses. So hadron masses are not additional input parameters in this effective field theory and come out automatically by considering chiral SU(3) symmetry, contrary to e.g. the standard relativistic mean-field theory (there is for example no explicit mass term for baryons in the Lagrangian!). The expressions for the baryon masses read for example

$$m_N^* = m_0 - \frac{1}{3} g_{O_8}^S (4\alpha_{OS} - 1) (\sqrt{2}\zeta - \sigma)$$

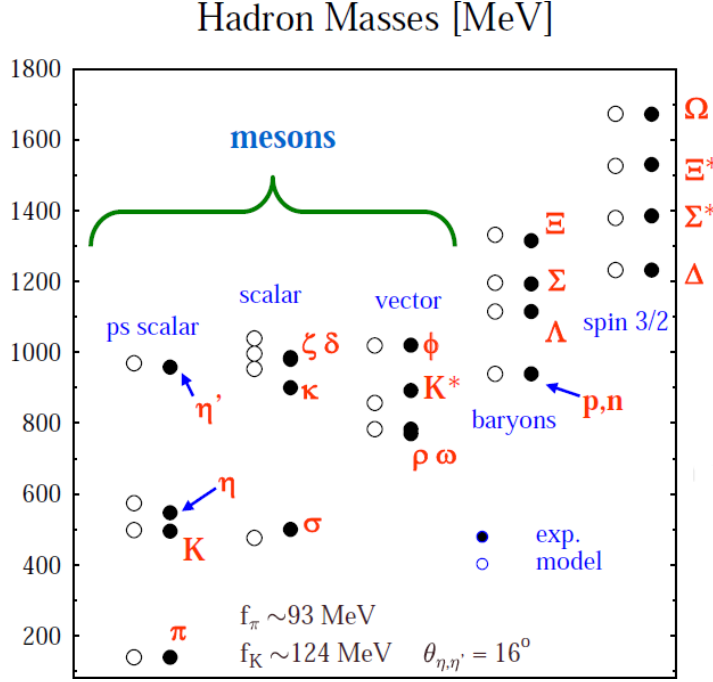


Fig. 1. – The hadron masses as generated by the vacuum expectation values of the chiral SU(3) model in comparison to the experimental data.

$$\begin{aligned}
 m_\Lambda^* &= m_0 - \frac{2}{3}g_{O8}^S(\alpha_{OS} - 1)(\sqrt{2}\zeta - \sigma) \\
 m_\Sigma^* &= m_0 + \frac{2}{3}g_{O8}^S(\alpha_{OS} - 1)(\sqrt{2}\zeta - \sigma) \\
 m_\Xi^* &= m_0 + \frac{1}{3}g_{O8}^S(2\alpha_{OS} + 1)(\sqrt{2}\zeta - \sigma)
 \end{aligned}
 \tag{9}$$

with  $m_0 = g_{O1}^S(\sqrt{2}\sigma + \zeta)/\sqrt{3}$ . The generated hadron mass spectrum is compared to the experimental data in Fig. 1.

For determining the necessary input to the Tolman-Oppenheimer-Volkoff (TOV) equation, the relation between pressure and energy density has to be calculated. The thermodynamic grandcanonical potential

$$\Omega/V = -\mathcal{L}_{\text{vec}} - \mathcal{L}_0 - \mathcal{L}_{\text{SB}} - \mathcal{V}_{\text{vac}} - \sum_i \frac{\gamma_i}{(2\pi)^3} \int d^3k [E_i^*(k) - \mu_i^*] - \frac{1}{3} \sum_l \frac{1}{\pi^2} \int \frac{dk k^4}{\sqrt{k^2 + m_l^2}}.$$

can be derived by standard methods. The particle energy of the baryons depends now

on the expectation values of the meson fields in the medium

$$(10) \quad E_i^*(k_i) = \sqrt{k_i^2 + m_i^{*2}}$$

so that the baryons acquire an effective mass  $m^*$  and an effective chemical potential

$$(11) \quad \mu_i = E_i^*(k_{F,i}) + g_{i\omega}\omega_0 + g_{i\phi}\phi_0 + g_{i\rho}I_{3i}\rho_0 ,$$

which is shifted by the vector potentials. All thermodynamic quantities, as the number density  $n$  and the energy density  $\epsilon$ , can be extracted from the thermodynamic potential via

$$(12) \quad p = -\frac{\Omega}{V} \quad , \quad n_i = \frac{\partial p}{\partial \mu_i} \quad , \quad \epsilon = -p + \sum_i \mu_i n_i \quad .$$

The coupling constants of the scalar mesons to the baryons are fixed by determining the baryon masses in vacuum. The vector coupling constant are automatically given by SU(3) symmetry relation:

$$(13) \quad g_{\Lambda\omega} = g_{\Sigma\omega} = 2g_{\Xi\omega} = \frac{2}{3}g_{N\omega} = 2g_{O8}^V; \quad g_{\Lambda\phi} = g_{\Sigma\phi} = \frac{g_{\Xi\phi}}{2} = \frac{\sqrt{2}}{3}g_{N\omega} .$$

which are actually the SU(6) symmetry relations known from the quark model (ideal mixing is assumed which is a very good approximation for the vector meson nonet).

The chiral effective model gives a good description of nuclear matter as well as of the properties of nuclei. The nuclear matter properties are a binding energy of  $E_B/A = -16$  MeV at  $n_0 = 0.15$  fm<sup>-3</sup> with an effective mass of  $m_N^*/m_N = 0.61$ , a compression modulus of  $K = 276$  MeV, and an asymmetry term of  $a_{\text{sym}} = 40.4$  MeV. Hyperons are automatically included by adopting consistently SU(3) symmetry for the chiral effective Lagrangian from the beginning. The computed single-particle energy levels of hypernuclei are depicted in Fig. 2 and compared with the experimental hypernuclear data. One sees an overall agreement with the data, just reflecting the fact that  $\Lambda$  hypernuclei are well described by a potential depth of the  $\Lambda$  at saturation density of about  $-30$  MeV. The situation for the other hyperons,  $\Sigma$  and  $\Xi$ , is far less clear. The  $\Sigma$  hypernuclear potential is likely to be repulsive, while there is experimental evidence that the  $\Xi$  hypernuclear potential is attractive, although significantly less in comparison to the one for  $\Lambda$  hyperons. In the chiral effective model, the hyperon potential are fixed already by the parameters and the SU(3) symmetry relations. The hyperon potential for the  $\Sigma$  comes out to be only barely repulsive in the chiral model, which will be important for the composition of neutron star matter.

Hyperons can appear in neutron star matter by virtue of the conditions of  $\beta$ -equilibrium [9, 10]. The timescale for weak interaction rates is of the order of  $10^{-10}$  s (decay timescale for hyperons) to  $10^{-8}$  s (decay timescale for kaons) in vacuum. In matter, similar rates are expected, as for example hyperons in hypernuclei have similar to just slightly smaller

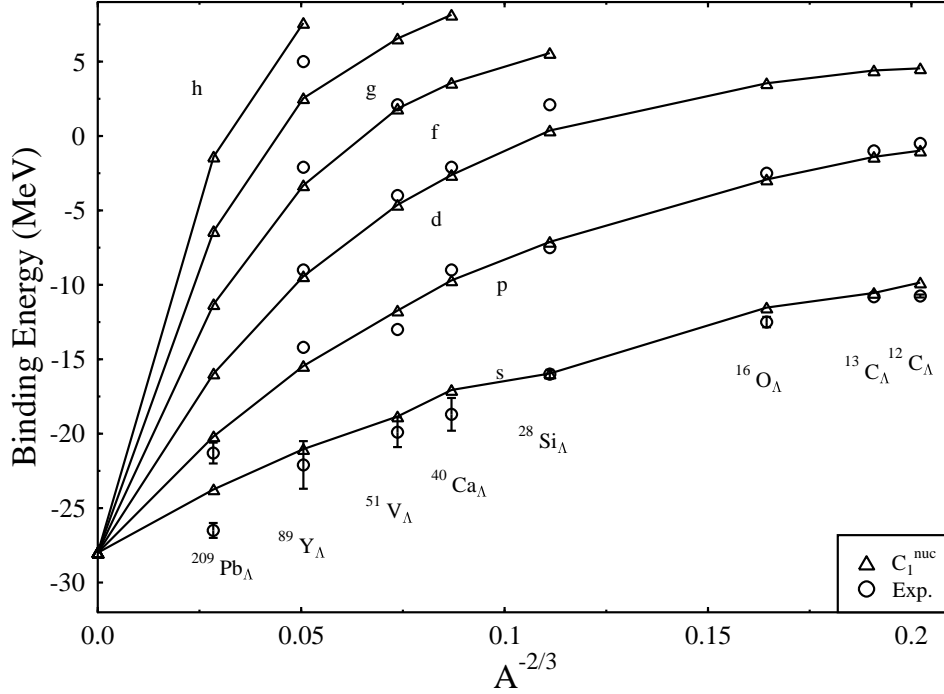


Fig. 2. – The single-particle energy levels of various hypernuclei for the SU(3) chiral model compared to the experimental data (taken from [7]).

lifetimes compared to the hyperon lifetime in vacuum. Neutron stars are known to be quite old, some of them have characteristic ages close to the age of the universe of  $10^{10}$  years, plenty of time to reach equilibrium for weak interactions,  $\beta$ -equilibrium. Hence,  $\Lambda$  hyperons can appear in dense neutron star matter if their effective energy in the medium reaches the baryochemical potential of neutrons at some baryon density  $n$ :  $E_{\Lambda}^*(n) = \mu_{\Lambda} = \mu_n$ . The relations between the chemical potentials of all particles are determined by the conserved charges of the particles, which for neutron star matter are just baryon number and charge (not strangeness, contrary to e.g. heavy-ion reactions). Hence, the chemical potential of all particles can be fixed by

$$(14) \quad \mu_i = B_i \cdot \mu_B + Q_i \cdot \mu_Q$$

where  $B_i$  and  $Q_i$  are the baryon number and the charge of the particle  $i$ , respectively. The effective energy for hyperons increases less rapidly than the one for nucleons, due to the SU(3) symmetry of the vector coupling constant of the vector potential, which dominates the high-density behaviour. Therefore, modern calculations of the composition

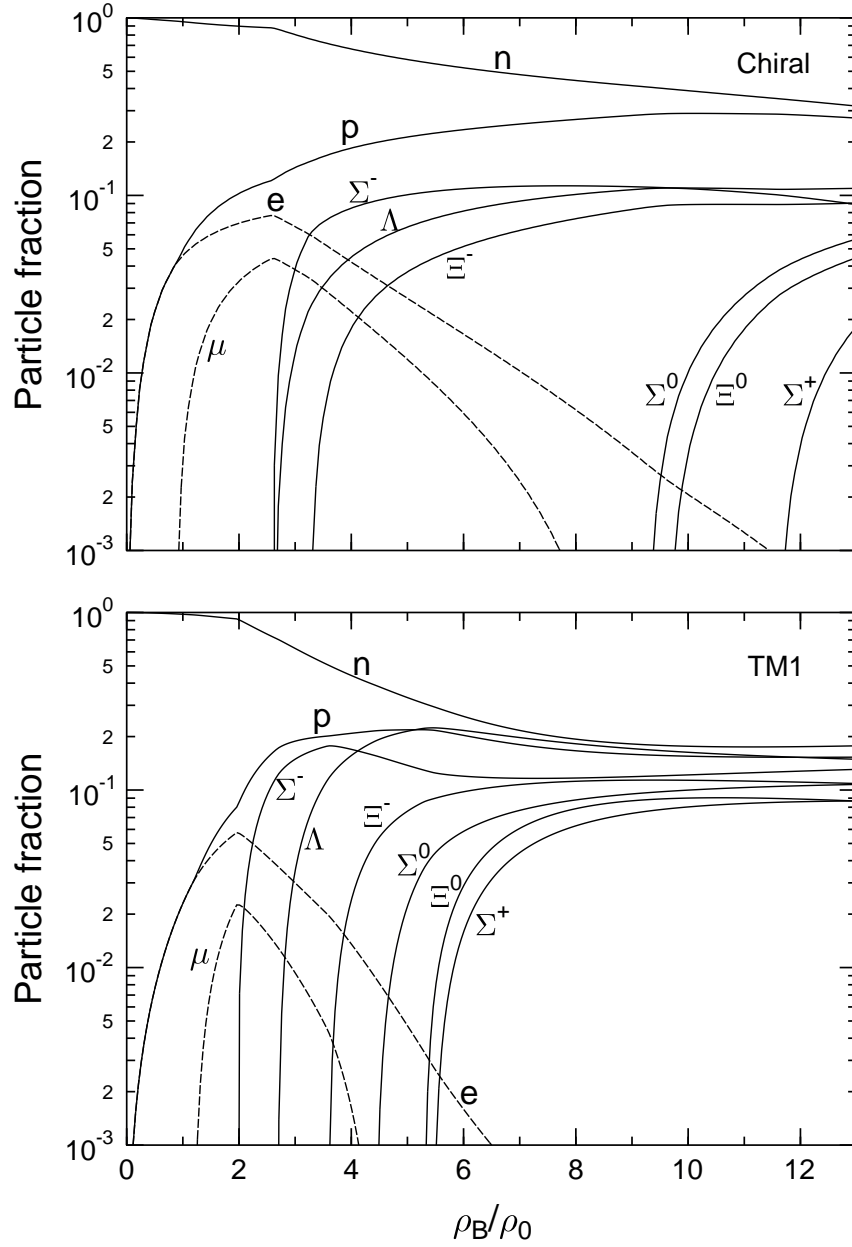


Fig. 3. – The composition of neutron star matter as a function of density for the chiral SU(3) model (upper plot) and the relativistic mean-field model using the parameter set TM1 (lower plot). Hyperons appear around twice normal nuclear matter density (taken from [8]).



of neutron star matter predict that hyperons appear around  $2n_0$ , where  $n_0$  stands for the normal nuclear matter density. Fig. 3 shows the composition as calculated from the chiral effective model presented above. Neutrons are the main component at low densities. Protons and electrons appear then with equal amounts, so as to conserve charge neutrality. Then at about  $2.5n_0$  first the  $\Sigma^-$  then the  $\Lambda$  hyperons are present in the matter, reaching fractions of around 10% at larger densities. The  $\Sigma^-$  appears before the  $\Lambda$  despite its heavier mass as negatively charged particles are favoured in neutron star matter, so as to balance the positive charge of the protons. The asymmetry energy of nucleons drives the system to isospin-neutral matter, i.e. equal amounts of neutrons and protons. Therefore, also the  $\Xi^-$  hyperons appears at lower densities than the  $\Xi^0$ , here slightly above  $3n_0$  already. For comparison, the composition for the standard relativistic mean-field (RMF) model is plotted also in Fig. 3. Here, equal hyperon potentials have been adopted for all hyperons. The pattern of the onset of hyperon populations is quite similar in the two models up to  $4n_0$ . For larger densities, the other hyperons are present at lower densities in the RMF model compared to the chiral model. However, the maximum density reached in neutron star configurations is about  $6n_0$ , so that the difference between those two models will be only important for the most massive neutron star configurations close to the maximum mass.

Hyperons have a dramatic effect on the nuclear equation of state (EoS), the relation between the pressure and the energy density of matter, which serves as the crucial input to the structure equations for compact stars, the Tolman-Oppenheimer-Volkoff equations. Fig. 4 shows the equation of state for the chiral model (thick lines) and the RMF model (thin lines). The upper curves are calculated with nucleons and leptons only, the lower ones include effects from the presence of hyperons in dense matter. One sees, that the hyperons substantially lower the pressure for a given energy density. This effect is stronger than the difference between the two models used here. In particular, the high-density EoS with hyperons is nearly the same in both models.

The lowering of the pressure has a destabilizing effect for neutron stars, as pressure is needed to counteract the attractive pull of gravity. Hence, one expects that the maximum possible mass for compact stars with hyperons is significantly lower than the one for neutron stars with just nucleons and leptons. Fig. 5 demonstrates this effect of hyperons on the mass-radius diagram of compact stars. Matter with nucleons and leptons only arrive at maximum masses of  $1.84M_\odot$  for the chiral and  $2.16M_\odot$  for the RMF model, respectively. The maximum masses with hyperons included are reduced to  $1.52M_\odot$  for the chiral and  $1.55M_\odot$  for the RMF model. Note, that the radii are different already at lower masses which is due to the difference in the EoS slightly above normal nuclear saturation density. The drastic reduction of the maximum mass due to hyperons is known to be a quite generic feature, see e.g. [11].

Finally, the transition to hyperon matter is studied by tuning up the hyperon-hyperon interaction, which is scarcely known from the few double  $\Lambda$  hypernuclear events available. With increasing hyperon-hyperon attraction, the transition to hyperons becomes a first order phase transition. The mixed phase, with slowly rising pressure as a function of energy density, will make the compact star less stable. The onset of the pure hyperonic

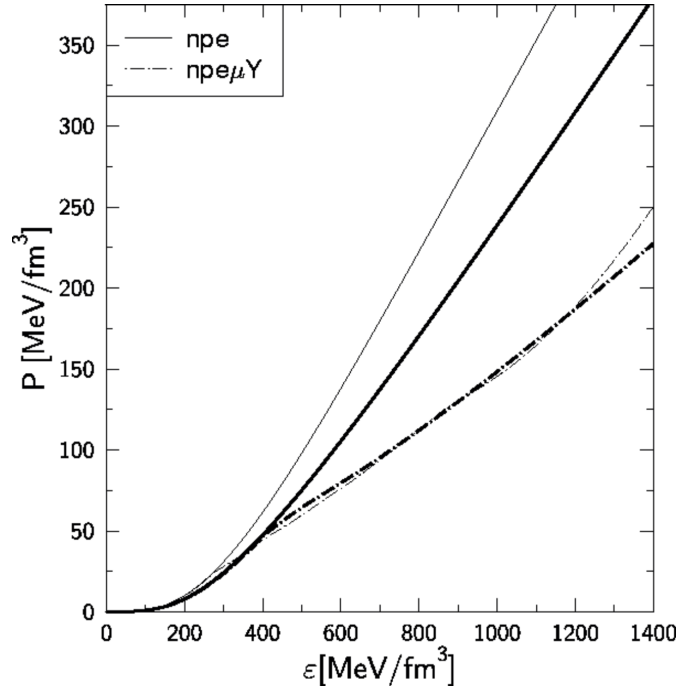


Fig. 4. – The equation of state of neutron star matter in  $\beta$ -equilibrium with and without hyperons (taken from [8]). Thick lines show the results for the chiral model, thin lines the ones for the RMF model using set TM1. Hyperons substantially reduce the pressure for a given energy density, i.e. they soften the equation of state.

phase with a steeply rising pressure can lead to another stable sequence of compact stars. For a sufficiently huge attraction between hyperons, hyperonic matter becomes more stable than pure nucleonic neutron star matter and the mass-radius relation changes to the one for selfbound stars, i.e. the mass increases from the origin with the radius as  $R^3$ , so that the average density in the star is nearly constant. Fig. 6 depicts the mass-radius diagram for an increased hyperon-hyperon attraction. For moderate attraction, the mass-radius relation has two distinct branches with correspondingly two maximum masses. The new branch at smaller radii is another stable solution to the TOV equations, constituting the so called third family of compact stars [13, 14]. For even larger hyperon attraction, the mass-radius relation changes to the one for selfbound stars: the mass-radius relation starts at the origin. Selfbound stars can still possess an outer nuclear crust, which is determined by the low-density nuclear EoS below neutron-drip density. In that case, the mass-radius relation for the low-mass configurations interpolates between the selfbound star configuration and the normal low-mass neutron star sequence.

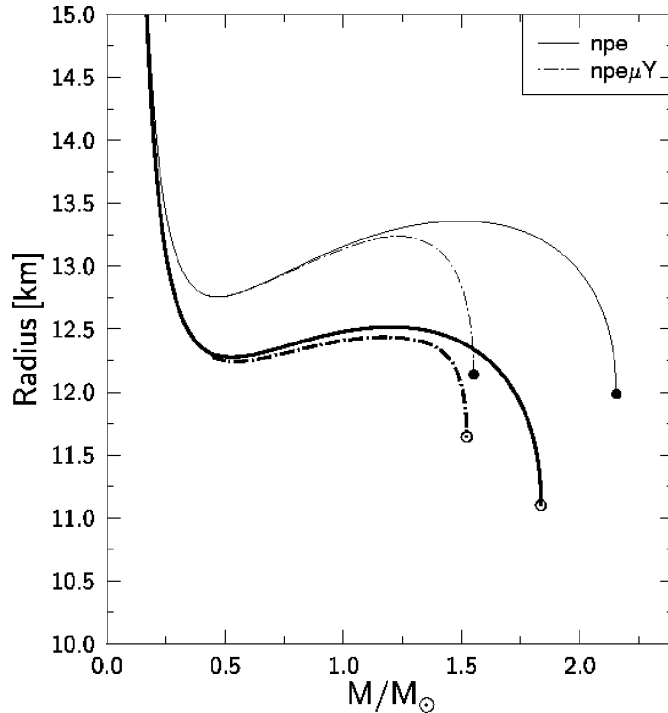


Fig. 5. – The mass-radius relation for the relativistic mean-field model using the parameter set TM1 (thin lines) and for the chiral SU(3) model (thick lines) with and without hyperons (taken from [8]). Hyperons substantially reduce the maximum possible mass.

### 3. – Strange Bosons in Hadron Stars

Besides hyperons, other hadronic particles can be present at high density in the core of neutron stars. In the following, we discuss how bosons and the phenomenon of Bose-Einstein condensation can be described in a simple relativistic field-theoretical approach, here for the case of kaon condensation in neutron star matter [15, 16]. We follow the field-theoretical model of Ref. [17, 18].

In dense matter, kaons, and in particular the negatively charged  $K^-$ , can appear in neutron star matter. For that to happen, it must be energetically favoured to replace electrons by  $K^-$  meson which translates to the condition that the effective energy of the  $K^-$  in the dense medium must be equal to the chemical potential of electrons,  $E_K^*(n) = \mu_e$ . The in-medium shift of the mass and the energy of the kaons can be modelled by Yukawa coupling terms to scalar and vector fields generated by the nuclear matter. Here, for simplicity, we adopt the standard relativistic mean-field model for the

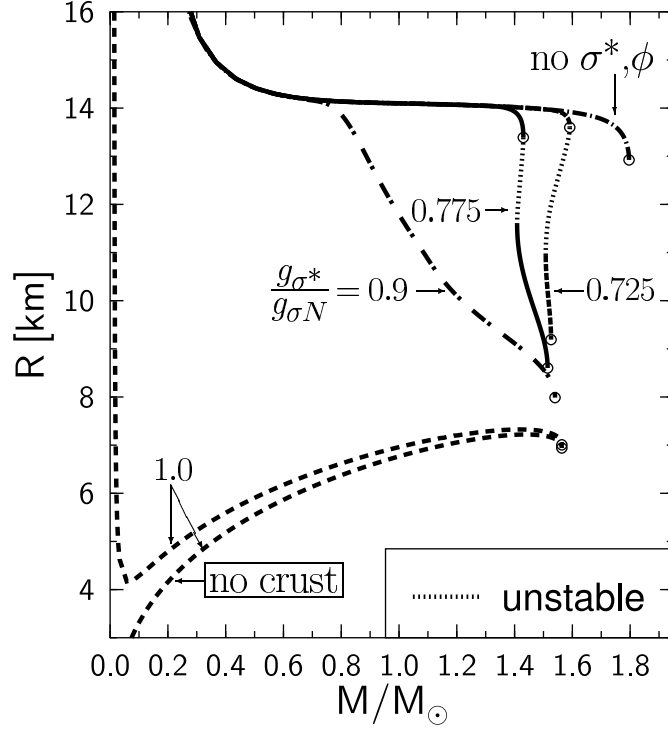


Fig. 6. – The mass-radius relation for different strength of the attractive hyperon-hyperon interactions as given by the coupling constant  $g_{\sigma^*}$  (taken from [12]). A new stable solution appears in the mass-radius relation with similar masses but smaller radii. Selfbound hyperon stars are shown by long-dashed lines.

nuclear part and just add those coupling terms for the kaon field to the Lagrangian:

$$\begin{aligned}
 \mathcal{L} = & \sum_B \bar{\Psi}_B \left( i\gamma_\mu \partial^\mu - m_B + g_{\sigma B} \sigma - g_{\omega B} \gamma_\mu V^\mu - g_{\rho B} \vec{\tau}_B \vec{R}_\mu \right) \Psi_B + \frac{1}{2} \partial_\mu \sigma \partial^\mu \sigma - \frac{1}{2} m_\sigma^2 \sigma^2 \\
 (15) \quad & -U(\sigma) - \frac{1}{4} V_{\mu\nu} V^{\mu\nu} + \frac{1}{2} m_\omega^2 V_\mu V^\mu + U(V) - \frac{1}{4} \vec{R}_{\mu\nu} \vec{R}^{\mu\nu} + \frac{1}{2} m_\rho^2 \vec{R}_\mu \vec{R}^\mu
 \end{aligned}$$

where the selfinteraction terms between the meson fields read

$$(16) \quad U(\sigma) = \frac{1}{3} b m (g_\sigma \sigma)^3 + \frac{1}{4} c (g_\sigma \sigma)^4, \quad U(V) = \frac{d}{4} (V_\mu V^\mu)^2.$$

If the critical condition for the onset of kaon condensation is fulfilled:

$$(17) \quad \omega_{K^-} = \mu_{K^-} = \mu_e$$

then processes like

$$(18) \quad e^- \rightarrow K^- + \nu_e \quad n \rightarrow p + K^-$$

produce kaons in the dense medium. The Lagrangian for the kaon field can be cast in the form

$$(19) \quad \mathcal{L}_K = \mathcal{D}_\mu^* K^* \mathcal{D}^\mu K - m_K^{*2} K^* K$$

where the vector fields are coupled minimally

$$(20) \quad \mathcal{D}_\mu = \partial_\mu + ig_{\omega K} V_\mu + ig_{\rho K} \vec{\tau}_K \vec{R}_\mu$$

and the effective mass of the kaon is defined as a linear shift of the mass term by the scalar field

$$(21) \quad m_K^* = m_K - g_{\sigma K} \sigma \quad .$$

The in-medium effective energy of the kaon can be read off from the energy-momentum relation by using a plane wave ansatz for the kaon field:

$$(22) \quad \omega_K = m_K - g_{\sigma K} \sigma - g_{\omega K} V_0 - g_{\rho K} R_{0,0} \quad .$$

The total energy density and pressure can be calculated with standard techniques from the energy-momentum tensor (assuming an ideal fluid), so that

$$(23) \quad \epsilon = \epsilon_N + \epsilon_K + \epsilon_{e,\mu}$$

$$(24) \quad p = p_N + p_{e,\mu} \quad .$$

The explicit expressions for the energy density originating from kaon condensation reads simply

$$(25) \quad \epsilon_K = m_K^* n_K \quad .$$

where  $n_K$  stands for the number density of kaons. Note, that there is no direct contribution from the kaon condensate to the pressure, as it vanishes for a Bose-Einstein condensate. Finally, one has to fix the coupling constants for the kaons. We adopt again symmetry arguments to relate the vector coupling constants for the kaons to the ones of the nucleon

$$(26) \quad g_{\omega K} = \frac{1}{3} g_{\omega N} \quad \text{and} \quad g_{\rho K} = g_{\rho N} \quad .$$

Here, the coupling to the vector mesons are assumed to be universal, which is the case when gauging the Lagrangian, so that the coupling constants are just related by isospin symmetry. An extension to SU(3) is straightforward, but not necessary here, as we

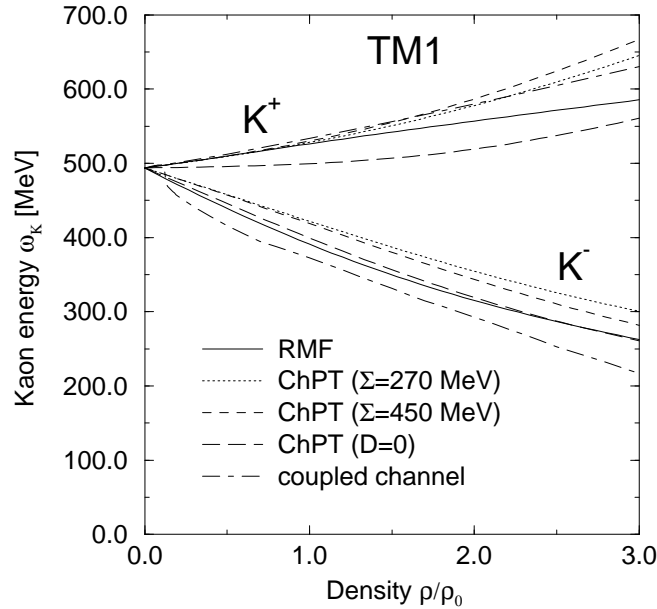


Fig. 7. – The kaon and antikaon energy in dense nuclear matter (taken from [24]). The kaon energy is shifted up, while the antikaon energy is greatly reduced as a function of density due to an overall strongly attractive antikaon-nucleon potential. RMF: relativistic mean-field model, ChPT: chiral perturbation theory with different values of the  $\Sigma$  term and for a vanishing range term,  $D = 0$  (see [24] for details).

discuss first neutron star matter with nucleons, leptons and kaons only and ignore the effects from hyperons. The scalar coupling constant can be related to the relativistic kaon in-medium potential via

$$(27) \quad U_K(\rho_0) = -g_{\sigma K}\sigma(\rho_0) - g_{\omega K}V_0(\rho_0)$$

which is a more appropriate (and pragmatic) control parameter. The kaon potential is not well known, but likely to be considerably attractive at high densities. Coupled channel calculations for kaons in dense matter arrive at values of up to  $-120$  MeV at normal nuclear matter density [19, 20, 21] although much shallower potentials are found in selfconsistent treatments, see e.g. [22, 23].

Fig. 7 shows the in-medium energy of kaons and antikaons as a function of baryon density for different approaches. The model outlined here is denoted by the label RMF. The prediction from the RMF approach are in good agreement with the one from chiral perturbation theory (ChPT), where several cases are shown but not discussed here in more details. The kaon energy is shifted up in the nuclear medium due to the repulsive

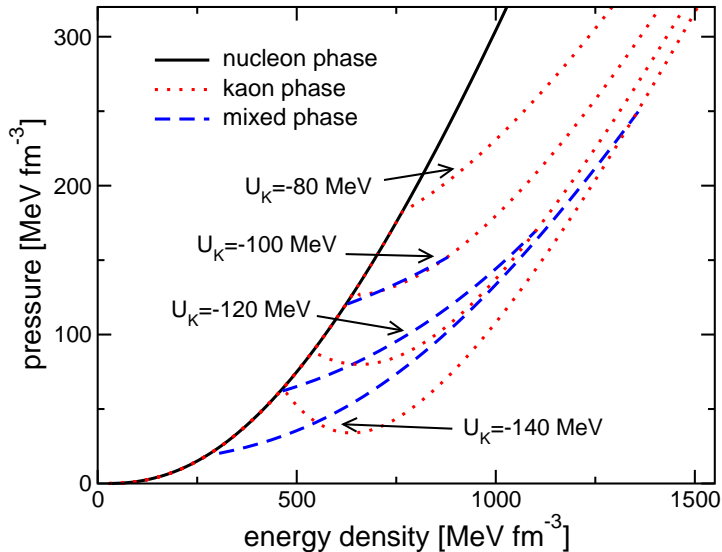


Fig. 8. – The equation of state for nucleon star matter with kaon condensation (from [18]). For large attractive kaon potentials, the transition to kaon condensation is of first order. The pressure decreases as function of energy density at the onset of kaon condensation (red dotted lines) indicating an instability. A Gibbs construction has to be used for the description of the mixed phase (blue dashed lines).

vector potential. The antikaon on the other hand experiences an attractive vector potential, so that the effective energy decreases dramatically as a function of density. For comparison, a coupled channel calculation for the  $K^-$  is also plotted, with rather similar results to the ones of the RMF model.

The appearance of kaon condensation in neutron star matter is accompanied by a strong first order phase transition. The Gibbs criteria for handling a phase transition with two conserved charges, baryon number and charge, states that the pressure in the two phases has to be equal for the same chemical potentials

$$(28) \quad p^I = p^{II}, \quad \mu_B^I = \mu_B^{II}, \quad \mu_e^I = \mu_e^{II}$$

The equation of state for neutron star matter is depicted in Fig. 8. The solid line stands for the purely nucleonic EoS, the dotted lines for the pure kaon condensed phase with nucleons and kaons for different values of the kaon potential. The pure kaon condensed phase is seen to be unstable, there is a region where the pressure decreases with increasing energy density. The Gibbs construction for the mixed phase of pure nucleon matter and pure kaon condensed matter (dashed lines) interpolates between the two phases in a thermodynamical consistent way, so that the pressure is continuously rising as a function

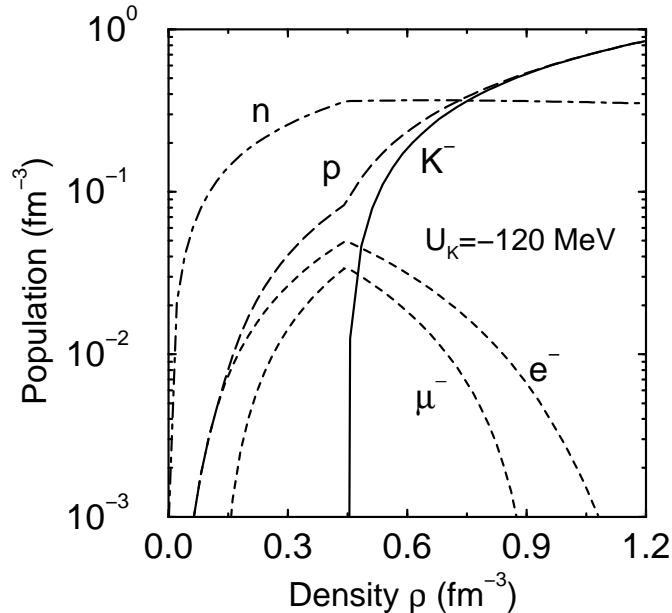


Fig. 9. – The population of nuclear star matter with kaon condensation for a kaon optical of  $U = -120$  MeV at  $n = n_0$  (taken from [18]). Kaons appear around  $3n_0$  and replace the electrons. The proton fraction balances the negative charge of the kaons and can be even larger than the neutron fraction for high densities.

of energy density.

The composition of neutron star matter with kaon condensation is shown in Fig. 9 for a kaon potential of  $U_K = -120$  MeV at  $n_0$ . The  $K^-$  set in at  $3n_0$  and reach a very high fraction already for slightly larger densities. As soon as the  $K^-$  are present, the electron and muon fraction decreases accordingly. At  $5n_0$  there are equal fractions of neutrons, protons and  $K^-$ , so neutron star matter would be more aptly called nucleon star matter. At even larger densities, the  $K^-$  dominate the population together with the protons, which ensures overall charge neutrality. The  $K^-$  in combination with protons are favoured in comparison to the neutrons as they are deeply bound in dense matter.

Fig. 10 depicts the corresponding mass-radius relation by using the equations of state as seen in Fig. 8. The lower the kaon optical potential, the lower is the critical density for the onset of kaon condensation. Hence, the mass-radius relation will deviate from the one of the canonical neutron star at lower masses for larger values of the kaon potential. As kaons are in a Bose-Einstein condensate and do not give a direct contribution to the pressure, less mass can be supported against the gravitational pull. For low values of the kaon potential, the mass-radius curve simply gets unstable as soon as kaons are part of the composition in the core of the compact star. For the case  $U_K = -130$  MeV, the mass slowly changes as a function of radius and very small radii well below 10 km are reached.



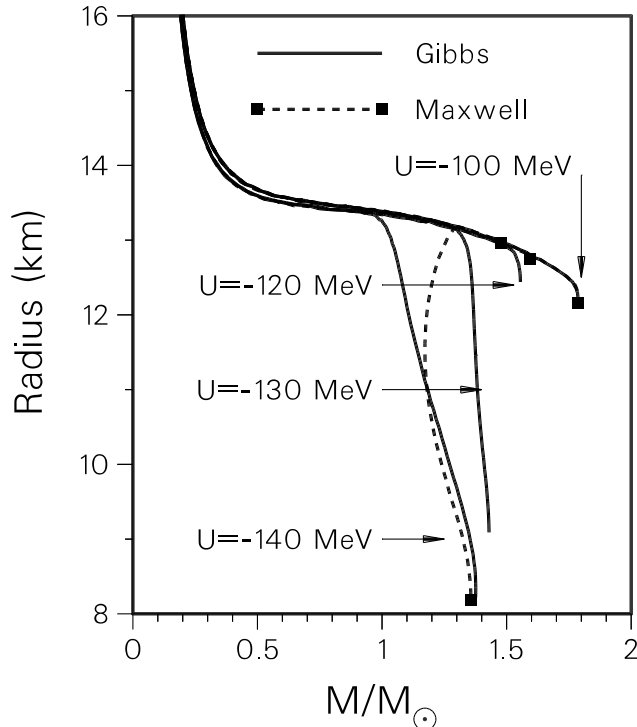


Fig. 10. – The mass-radius relation for kaon-condensed nucleon stars (taken from [18]). The maximum mass is reduced and extremely small radii of about 8 km are possible when kaon condensation is present.

High compression is needed to stabilise a kaon condensate compact star. For even more attraction, the case  $U_K = -140$  MeV, there appears a significant difference in the mass-radius curves between the (thermodynamically inconsistent) Maxwell construction and the Gibbs construction. A strong first order phase transition is present in the core of the compact star from neutron star matter to kaon condensed star matter. Interestingly, the deviations in the mass-radius curve due to the different descriptions of the mixed phase remains to be just in some intermediate region of the mass-radius curve. For the last sequence of stable compact star configuration up to the maximum mass, the two descriptions give about similar results for the mass-radius curve. The unstable region in the case of the Maxwell construction, indicated by a change of the slope of the mass-radius diagram, is absent in the case of the Gibbs construction. Note, that for the Gibbs construction, the kaon condensed phase appears at much lower values of the mass of the compact star compared to the Maxwell construction. We will discuss phase transitions in more detail with regard to the onset of the quark matter phase at high densities, to which we turn now.

#### 4. – Strange Quark Matter in Compact Stars

In this section, we discuss the properties of compact stars with quark matter. First, pure quark stars are addressed and the mass-radius diagram for so-called selfbound stars. Then, the quark matter equation of state is matched to the one of the low-density hadronic equation of state. Compact stars with both types of matter, hadronic and quark matter, are dubbed hybrid stars.

**4.1. General properties of quark stars.** – QCD predicts that quarks at large energy scales are asymptotically free. For high energy-density matter one considers a gas of free quarks with corrections from one-gluon exchange. The pressure at zero temperature and finite quark-chemical potential  $\mu$  reads for massless quarks

$$(29) \quad p(\mu) = \frac{N_f \mu^4}{4\pi^2} \left\{ 1 - 2 \left( \frac{\alpha_s}{\pi} \right) - \left[ G + N_f \ln \frac{\alpha_s}{\pi} + \left( 11 - \frac{2}{3} N_f \right) \ln \frac{\bar{\Lambda}}{\mu} \right] \left( \frac{\alpha_s}{\pi} \right)^2 \right\}$$

where  $N_f$  stands for the number of flavours (here  $N_f = 3$ ). The constant  $G$  is scheme dependent and in the  $\overline{\text{MS}}$  scheme given by  $G = G_0 - 0.536 N_f + N_f \ln N_f$ ,  $G_0 = 10.374 \pm 0.13$  [25]. The renormalisation scale  $\Lambda$  will be fixed to be proportional to the quark-chemical potential. The expression for the pressure of massive quarks can be found in [26].

In compact star matter, weak reactions are in equilibrium so that

$$(30) \quad \begin{aligned} d &\longrightarrow u + e^- + \bar{\nu}_{e^-}, \\ s &\longrightarrow u + e^- + \bar{\nu}_{e^-}, \\ s + u &\longleftrightarrow d + u, \end{aligned}$$

and the chemical potentials for down and strange quarks must be equal, while the one for up quarks is just shifted by the electrochemical potential:

$$(31) \quad \mu_s = \mu_d = \mu_u + \mu_e.$$

Note, that this amounts to baryon and charge number conservation, the chemical potentials of the quarks can be also expressed in terms of the baryochemical potential and the electrochemical, as done in the previous sections. This fact will be beneficial for our discussion of the matching of the two phases in the next subsection, for example the connection  $\mu_n \equiv \mu_u + 2\mu_d$  can then be easily made. From the pressure one can compute the number density  $n$  and energy density  $\epsilon$  via the standard thermodynamic relations for each quark separately

$$(32) \quad n_f(\mu_f) = \frac{dp_f(\mu_f)}{d\mu_f} \quad \text{and} \quad \epsilon_f(\mu_f) = -p_f(\mu_f) + \mu_f \rho_f(\mu_f).$$

In addition, pure quark star matter should be charge neutral so that for the total charge density

$$(33) \quad n_c = \frac{2}{3}n_u - \frac{1}{3}n_d - \frac{1}{3}n_s - n_e = 0$$

where  $n_i$  stands for the number density of the species  $i$ . Finally, the total energy density and pressure of the quark matter is

$$(34) \quad \epsilon_Q = \epsilon_u + \epsilon_d + \epsilon_s + \epsilon_e,$$

$$(35) \quad p_Q = p_u + p_d + p_s + p_e \quad .$$

For comparison, one arrives at the MIT bag model by setting the coupling constant to zero and shifting the energy density and pressure of the quark matter by the bag constant  $B$  which describes the non-perturbative aspects of the QCD vacuum:

$$(36) \quad \epsilon_{\text{bag}} = \epsilon_{\text{free}} + B \quad p_{\text{bag}} = p_{\text{free}} - B$$

which can be combined to

$$(37) \quad p_{\text{bag}} = \frac{1}{3}\epsilon_{\text{bag}} - \frac{4}{3}B$$

as  $p_{\text{free}} = \epsilon_{\text{free}}/3$ .

In the following we consider quark matter of massless up, down, and strange quarks. The current strange quark mass of about 100 MeV is smaller than the scale of the quark-chemical potential of 300 MeV and more. Corrections are of the order of  $(m_s/\mu)^2$  and can be safely ignored for our purposes. For the case of three-flavour massless quarks quark matter consists of equal number densities of up, down and strange quarks and is charge neutral by itself. Hence, there are no electrons in such idealised quark matter (in fact the corrections from the finite strange quark mass are small). The chemical potentials of all three quark species are the same and just given by the quark-chemical potential. The quark number density and the energy density is then determined by

$$(38) \quad n = \frac{dp}{d\mu} \quad \epsilon = -p + \mu \cdot n$$

which fixes the quark matter equation of state in parametric form. The pressure actually vanishes for some critical chemical potential. Hence, there is a energy density jump from the vacuum to the energy density of quark matter. Pure quark matter is then stable at this characteristic energy density. This feature of the quark matter equation of state can be easily seen for the MIT bag model but is also present in the interacting model. The characteristic energy density is then fixed by the bag constant, as  $\epsilon_{\text{bag}} = 4B$  for vanishing pressure.

Fig. 11 depicts the mass-radius relation for compact stars consisting of pure quark matter. The solid lines show the interacting case for the perturbative QCD equation of

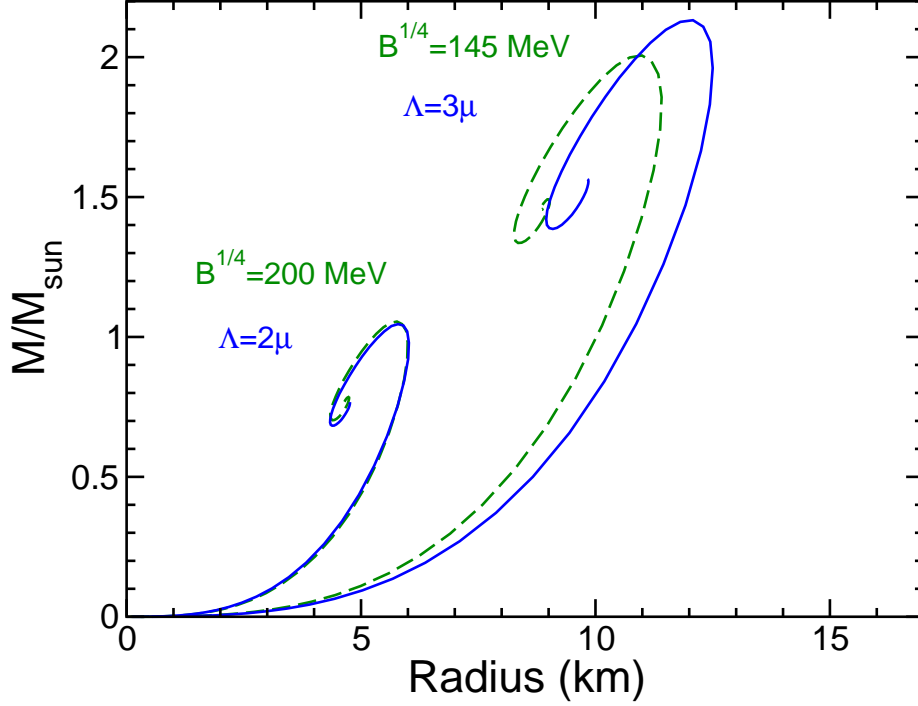


Fig. 11. – The mass-radius relation of pure quark stars in two different approaches: for the MIT bag model (green dashed curves) and within perturbative QCD calculation (blue solid lines). The general form of the mass-radius relation is remarkably similar.

state, the dashed line the one for the MIT bag model for so-called strange stars [27, 28]. As the pressure vanishes at some finite value of the energy density, the quark stars are stabilised and have about similar densities. Hence, the mass increases with the radius of the quark star as  $R^3$  starting at the origin. There is a maximum mass, as at some critical number of quarks the gravitational pull can not be counteracted by the Fermi pressure. The curves can be scaled into each other. For the MIT bag model, maximum mass and the corresponding radius scale as  $B^{-1/2}$ , smaller values of the MIT bag constant give larger maximum masses and larger radii. The result for the perturbative QCD model are strikingly close to the simple MIT bag model. Here larger choices for the renormalisation scale result in larger maximum masses and radii. Note, that pure quark stars can only exist if strange quark matter is more stable than ordinary nuclear matter, so that any hadronic mantle is transformed to strange quark matter, which is the so-called Bodmer-Witten hypothesis [29, 30].

4.2. *Hybrid stars: compact stars with quark and hadron matter.* – It is more likely that strange quark matter is not absolutely stable, so that the quark core is surrounded

by hadronic matter. The compact star is then dubbed a hybrid star. The transition from one phase to the other in compact star matter has to be modelled via the Gibbs condition for phase transitions [31] which states that in phase equilibrium the pressure of the two phases is the same for the same chemical potentials of the two phases

$$(39) \quad p_H(\mu_B, \mu_e) = p_Q(\mu_B, \mu_e).$$

Here, the index  $Q$  denotes the quantity in the quark phase,  $H$  the one in the hadronic phase. There are two conserved charges for compact star matter, the baryon number and charge, so that there are two independent chemical potentials. A Maxwell construction could only ensure that one chemical potential is continuous throughout the phase transition while the other would jump discontinuously. The volume fraction of the quark phase

$$(40) \quad \chi = \frac{V_Q}{V_Q + V_H}$$

can be used to calculate the total energy density in the mixed phase

$$(41) \quad \epsilon_{mix} = \chi \epsilon_Q + (1 - \chi) \epsilon_H.$$

The charge neutrality is now guaranteed globally, i.e. the Gibbs construction allows for highly charged phases whose charges balance each other.

The Gibbs construction can be visualised by the intersection of the two planes in a diagram where the pressure is plotted as a function of the two chemical potentials, see Fig. 12. In the plane of the pressures there is one line which indicates locally charge neutral matter of a single component, quark or hadron matter. The line of the intersection of the two pressure planes defines the mixed phase, the pressure is equal in the two phases. One realizes that the line of intersection is off the line of charge neutral matter for the quark or the hadron phase alone. The volume fraction is now chosen in such a manner that the total mixed phase has a vanishing charge density  $\rho$  and is charge neutral globally:

$$(42) \quad \rho_{mix} = \chi \rho_Q + (1 - \chi) \rho_H = 0.$$

At the beginning of the mixed phase, highly negative charged quark matter bubbles appear while hadron matter is slightly positively charged. At the end of the mixed phase, quark matter is slightly negative charged while there are small bubbles of highly positive charged hadron matter. This mismatch of charges is energetically favoured, hadron matter is more stable for about equal numbers of protons and neutrons due to the asymmetry energy, so that a positive charge is advantageous.

The corresponding composition for hybrid stars is depicted in Fig. 13 as a function of the radius for different choices of the MIT bag constant. For low values of the bag constant, the core consists of pure quark matter which can be the dominant part in the overall composition of the hybrid star. A sizable mixed phase exists, in particular for

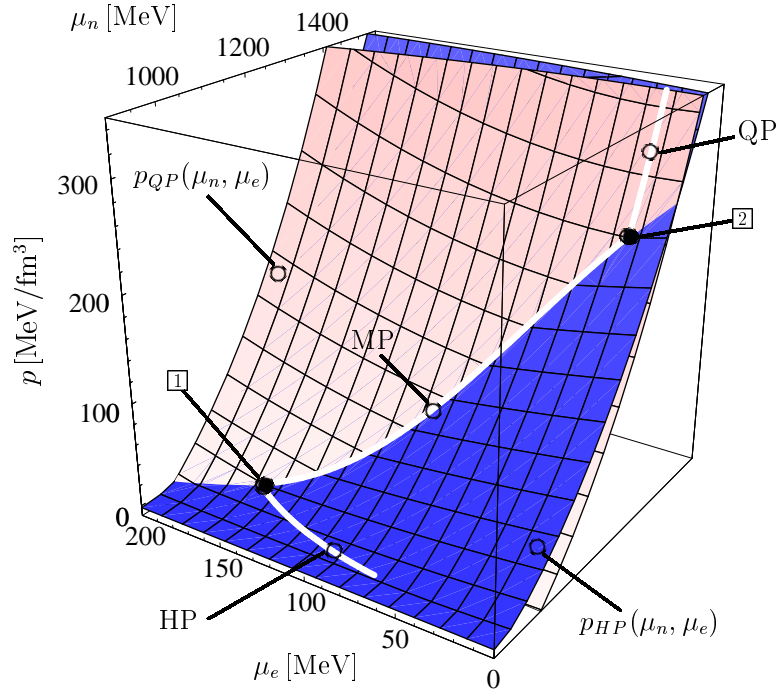


Fig. 12. – The Gibbs phase construction for two chemical potentials by looking at the pressure in 3D. The surface of the hadronic pressure cuts the one of the quark matter pressure along the phase coexistence line where both pressures are equal. The overall charge neutrality condition fixes a line in the hadronic pressure area and also in the quark one. Charge neutrality is ensured along the mixed phase line by adjusting the volume fractions of hadron and quark matter (taken from [14]).

large values of the bag constant, where the pure quark core is absent in the hybrid star. For sufficiently large values of the bag constant, the mixed phase as well as the pure quark phase is not present in the compact star, which is then an ordinary neutron star without any quark matter component in its core. The right plot shows the case, when the quarks have a quasiparticle effective mass due to interactions via gluon exchange which is parameterised by the coupling constant  $g$ . The onset of the mixed phase and the pure quark phase is shifted to lower values of the bag constant. Note, that the composition of a compact star with quark matter is highly sensitive to the choice of the bag constant. Anything between a pure quark star and an ordinary compact star of hadronic matter only is possible due to our present limited knowledge about the properties of quark matter at extreme densities.

Finally, the mass-radius diagram for hybrid stars is shown in Fig. 14 for different values of the bag constant. For large radii, a mixed phase is formed in the core of the compact star. The mass is decreasing for lower values of the bag constant (note the small differences in the values for the bag constant). For some values of the bag constant, the

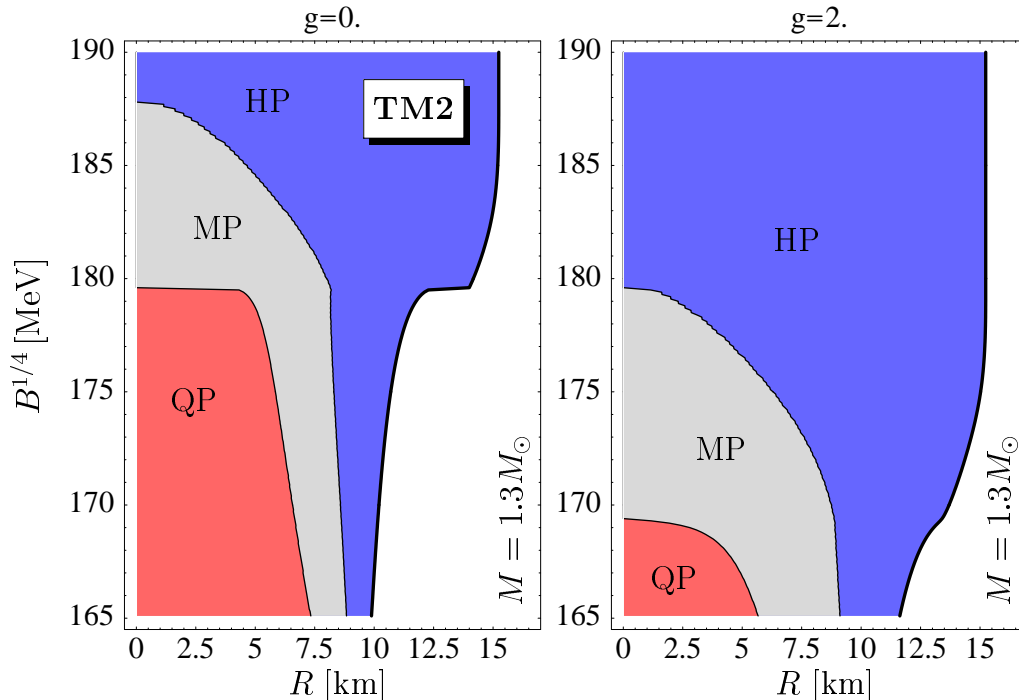


Fig. 13. – The composition of hybrid stars for different values of the MIT bag constant  $B$  (taken from [14]). For large values of  $B$ , the compact star is purely hadronic. A pure quark core is present for small values of  $B$ . Note, that for even lower values of  $B$ , the pure quark phase will extend up to the surface of the compact star and a pure quark star (a so called strange star) is formed.

mass decreases as a function of the central energy density (for smaller radii) after reaching a maximum mass. This region is unstable with respect to radial oscillations. However, at even larger central energy densities (smaller radii), the mass starts to increase again and a new sequence of stable solutions appear. The compact stars corresponding to these new stable sequence constitute a third family of compact stars, besides white dwarfs and ordinary neutron stars. They are stabilised by the presence of a pure quark phase which has a sufficiently stiff equation of state so as to support very dense compact star configurations. It is possible to have two compact stars with identical masses but with different radii, so-called compact star twins [13, 14].

In recent years, the properties of QCD at high densities have been explored in connection with the phenomenon of colour-superconductivity [32, 33], for reviews see e.g. [34, 35]. A rich phase structure exists in the QCD phase diagram at high densities and low temperatures right in the regime of compact star physics. In particular, several phase transitions might be present in compact star matter, so that the quark matter core of hybrid stars might contain more than one phase transition. This research field

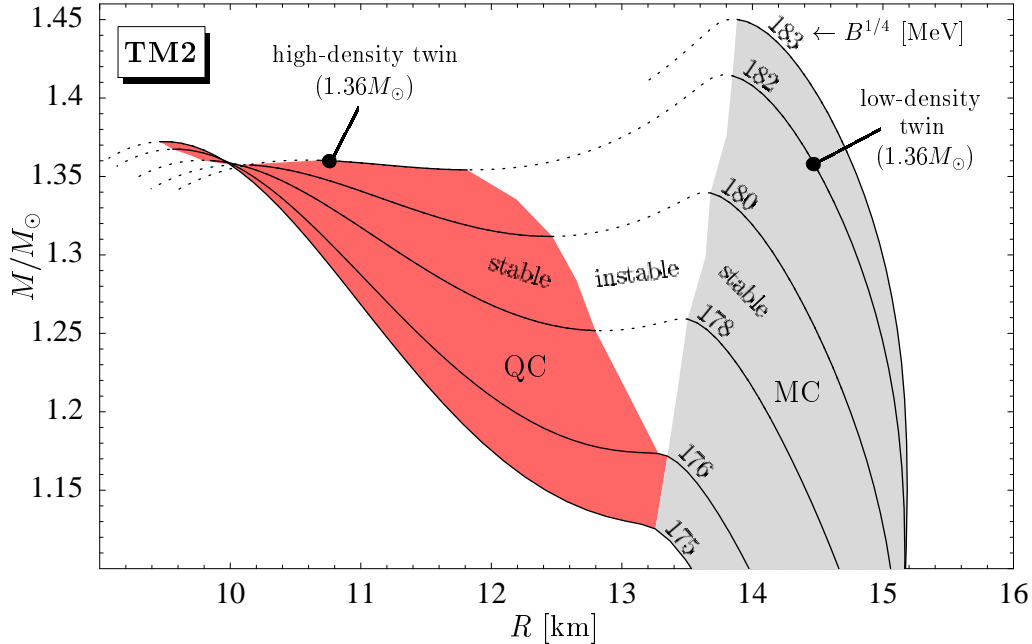


Fig. 14. – The mass-radius relation of hybrid stars, compact stars with hadronic and quark matter (taken from [14]). Configurations exist where the core consists just of the mixed phase (mixed core: MC) or where the core contains pure quark matter (quark core: QC). In the latter case, the compact star with a quark core can constitute a third family of compact stars with similar masses but smaller radii than the mixed core counterparts.

is rapidly evolving and is poised for new discoveries for the properties of compact stars with quark matter. We refer the interested reader to the above mentioned review articles for further reading.

## 5. – Summary

Compact stars can have a rich structure with new and exotic phases being present in their cores. Hyperons, heavy baryons with strangeness, can appear in neutron star matter. As a new fermionic degree of freedom, hyperons lower the overall pressure so that the maximum mass of a compact star with hyperons is substantially smaller than the one of a neutron star consisting of nucleons and leptons only. Also, negatively charged Bose-Einstein condensate could be formed via kaon condensation at high densities. As the Bose-Einstein condensate does not give a direct contribution to the pressure of the system, the stable sequence of compact stars in the mass-radius diagram simply stops as soon as the kaon condensed phase appears or extremely dense compact stars are generated with unusually small radii. Finally, at high densities quark matter can be present. Depending on the onset of the phase transition and the strength of the first-



order phase transition from the hadronic to the quark matter phase, a third family of compact stars is found in the mass-radius diagram. The compact stars of this third family have a core of pure quark matter and smaller radii than ordinary hybrid stars. The physics of dense quark matter in compact star opens exciting new perspectives in exploring the phase diagram of QCD at high densities. The new research facility FAIR at GSI Darmstadt will explore this fascinating regime of strong interaction physics in the near future with relativistic heavy-ion collisions with bombarding energies tuned so as to create compressed baryonic matter at highest baryon densities.

## REFERENCES

- [1] L. D. Landau, *Physik. Zeits. Sowjetunion* **1**, 285 (1932).
- [2] N. K. Glendenning, *Compact Stars — Nuclear Physics, Particle Physics, and General Relativity* (Springer, New York, 2000), 2nd ed.
- [3] F. Weber, *Pulsars as Astrophysical Laboratories for Nuclear and Particle Physics* (Institute of Physics, Bristol, 1999).
- [4] P. Hansel, A. Y. Potekhin, and D. G. Yakovlev, *Neutron Stars 1 : Equation of State and Structure*, vol. 326 of *Astrophysics and Space Science Library* (Springer, New York, 2007).
- [5] J. M. Lattimer and M. Prakash, *Phys. Rept.* **442**, 109 (2007), astro-ph/0612440.
- [6] J. M. Lattimer and M. Prakash, *Science* **304**, 536 (2004), astro-ph/0405262.
- [7] C. Beckmann *et al.*, *Phys. Rev. C* **65**, 024301 (2002), nucl-th/0106014.
- [8] M. Hanauske, D. Zschesche, S. Pal, S. Schramm, H. Stöcker, and W. Greiner, *Astrophys. J.* **537**, 958 (2000), arXiv:astro-ph/9909052.
- [9] V. A. Ambartsumyan and G. S. Saakyan, *Sov. Astron.* **4**, 187 (1960).
- [10] N. K. Glendenning, *Astrophys. J.* **293**, 470 (1985).
- [11] N. K. Glendenning and S. A. Moszkowski, *Phys. Rev. Lett.* **67**, 2414 (1991).
- [12] J. Schaffner-Bielich, M. Hanauske, H. Stöcker, and W. Greiner, *Phys. Rev. Lett.* **89**, 171101 (2002), astro-ph/0005490.
- [13] N. K. Glendenning and C. Kettner, *Astron. Astrophys.* **353**, L9 (2000), astro-ph/9807155.
- [14] K. Schertler, C. Greiner, J. Schaffner-Bielich, and M. H. Thoma, *Nucl. Phys.* **A677**, 463 (2000), astro-ph/0001467.
- [15] D. B. Kaplan and A. E. Nelson, *Phys. Lett.* **B175**, 57 (1986).
- [16] G. E. Brown, K. Kubodera, M. Rho, and V. Thorsson, *Phys. Lett. B* **291**, 355 (1992).
- [17] N. K. Glendenning and J. Schaffner-Bielich, *Phys. Rev. Lett.* **81**, 4564 (1998).
- [18] N. K. Glendenning and J. Schaffner-Bielich, *Phys. Rev. C* **60**, 025803 (1999).
- [19] V. Koch, *Phys. Lett. B* **337**, 7 (1994).
- [20] T. Waas, N. Kaiser, and W. Weise, *Phys. Lett. B* **379**, 34 (1996).
- [21] L. Tolos, A. Ramos, A. Polls, and T. T. S. Kuo, *Nucl. Phys.* **A690**, 547 (2001).
- [22] M. Lutz, *Phys. Lett. B* **426**, 12 (1998).
- [23] L. Tolos, A. Ramos, and E. Oset, *Phys. Rev. C* **74**, 015203 (2006), nucl-th/0603033.
- [24] J. Schaffner-Bielich, I. N. Mishustin, and J. Bondorf, *Nucl. Phys.* **A625**, 325 (1997), nucl-th/9607058.
- [25] E. S. Fraga, R. D. Pisarski, and J. Schaffner-Bielich, *Phys. Rev. D* **63**, 121702(R) (2001), hep-ph/0101143.
- [26] E. S. Fraga and P. Romatschke, *Phys. Rev.* **D71**, 105014 (2005), hep-ph/0412298.
- [27] P. Haensel, J. L. Zdunik, and R. Schaeffer, *Astron. Astrophys.* **160**, 121 (1986).
- [28] C. Alcock, E. Farhi, and A. Olinto, *Astrophys. J.* **310**, 261 (1986).

- [29] A. R. Bodmer, *Phys. Rev. D* **4**, 1601 (1971).
- [30] E. Witten, *Phys. Rev. D* **30**, 272 (1984).
- [31] N. K. Glendenning, *Phys. Rev. D* **46**, 1274 (1992).
- [32] M. Alford, K. Rajagopal, and F. Wilczek, *Phys. Lett. B* **422**, 247 (1998), hep-ph/9711395.
- [33] R. Rapp, T. Schäfer, E. V. Shuryak, and M. Velkovsky, *Phys. Rev. Lett.* **81**, 53 (1998), hep-ph/9711396.
- [34] D. H. Rischke, *Prog. Part. Nucl. Phys.* **52**, 197 (2004).
- [35] M. G. Alford, A. Schmitt, K. Rajagopal, and T. Schäfer, arXiv:0709.4635 [hep-ph] (2007).